10-16-2024

Rootzone Soil Moisture Dynamics Using Terrestrial Water-Energy Coupling

Vinit Sehgal
Department of Biological and Agricultural Engineering

Binayak P. Mohanty
Department of Biological and Agricultural Engineering

Rolf H. Reichle
NASA Goddard Space Flight Center

AGU ADVANCING EARTH AND SPACE SCIENCES

Geophysical Research Letters

RESEARCH LETTER
10.1029/2024GL110342

Special Collection:
Land-atmosphere coupling: measurement, modelling and analysis

Key Points:

- Terrestrial water-energy coupling is used to parameterize low-pass filter to estimate rootzone dynamics from surface soil moisture
- Rootzone degree of saturation and water-energy coupling thresholds are estimated using evaporative fraction and surface soil moisture
- SMAP-based rootzone degree of saturation can used for operational, near-real-time agricultural drought monitoring over Contiguous U.S

Supporting Information:

Supporting Information may be found in the online version of this article.

Correspondence to:
B. P. Mohanty,
bmohanty@tamu.edu

Citation:
Sehgal, V., Mohanty, B. P., & Reichle, R. H. (2024). Rootzone soil moisture dynamics using terrestrial water-energy coupling. *Geophysical Research Letters*, *51*, e2024GL110342. https://doi.org/10.1029/2024GL110342

Received 17 MAY 2024
Accepted 8 SEP 2024

Author Contributions:
Conceptualization: Vinit Sehgal, Binayak P. Mohanty, Rolf H. Reichle
Data curation: Vinit Sehgal
Formal analysis: Vinit Sehgal, Binayak P. Mohanty
Funding acquisition: Binayak P. Mohanty
Investigation: Vinit Sehgal, Binayak P. Mohanty

Rootzone Soil Moisture Dynamics Using Terrestrial Water-Energy Coupling

Vinit Sehgal[1,2,3], Binayak P. Mohanty[1], and Rolf H. Reichle[4]

[1]Biological and Agricultural Engineering, Texas A&M University, College Station, TX, USA, [2]Water Management and Hydrological Science, Texas A&M University, College Station, TX, USA, [3]Now at the School of Plant, Environmental, and Soil Sciences, Louisiana State University, Baton Rouge, LA, USA, [4]Global Modeling and Assimilation Office, NASA Goddard Space Flight Center, Greenbelt, MD, USA

Abstract A lack of high-density rootzone soil moisture (θ_{RZ}) observations limits the estimation of continental-scale, space-time contiguous θ_{RZ} dynamics. We derive a proxy of daily θ_{RZ} dynamics — *active* rootzone degree of saturation (S_{RZ}) — by recursive low-pass (LP) filtering of surface soil moisture (θ_S) within a terrestrial water-energy coupling (WEC) framework. We estimate the LP filter parameters and WEC thresholds for the piecewise-linear coupling between S_{RZ} and evaporative fraction (EF) at remote sensing and field scale over the Contiguous U.S. We use θ_S from the Soil Moisture Active-Passive (SMAP) satellite and 218 in-situ stations, with EF from the Moderate Resolution Imaging Spectroradiometer. The estimated S_{RZ} compares well against SMAP Level-4 estimates and in-situ θ_{RZ}, at the corresponding scale. The instantaneous hydrologic state (S_{RZ}) vis-à-vis the WEC thresholds is proposed as a rootzone soil moisture stress index (SMS_{RZ}) for near-real-time operational agricultural drought monitoring and agrees well with established drought metrics.

Plain Language Summary Rootzone soil moisture plays a vital role in agricultural, hydrological, and ecosystem processes. The available spaceborne satellites for monitoring soil moisture can only capture variability in a shallow soil layer at the surface, typically limited to the top 5 cm. Hence, spatiotemporally continuous estimation of rootzone soil moisture dynamics typically relies on soil moisture estimates from land-surface models, which are subject to errors in the surface meteorological forcing data, process formulations, and model parameters. Some studies suggest that the rootzone soil moisture dynamics can be estimated by filtering the high-frequency variability in the surface soil moisture. However, such "*filters*" require observed rootzone data (often unavailable at high spatial density) for calibration. This study uses the relationship between surface soil moisture and evaporative fraction derived using spaceborne observations from the Soil Moisture Active Passive mission and the Moderate Resolution Imaging Spectroradiometer to estimate rootzone soil moisture dynamics for the Contiguous U.S. at 9 km grid resolution. We further demonstrate that this approach can be extended into a near-real-time agricultural drought monitor to assess drought impacts on vegetation using surface soil moisture observations.

1. Introduction

Dynamic soil-vegetation-atmosphere interactions are manifested in the space-time variability of the active rootzone soil moisture (θ_{RZ}), thereby governing several ecohydrological processes such as watershed-scale streamflow generation (Koster et al., 2023), nutrient recycling and soil microbial activities (Li et al., 2021; Wang et al., 2017), terrestrial carbon fluxes (Lin et al., 2019; Raghav & Kumar, 2021; Sebastian et al., 2023), and groundwater recharge (Dash et al., 2019). However, long-term space-time-contiguous studies of θ_{RZ} dynamics at the continental scale typically rely on land-surface models (LSMs) owing to the shallow penetration depth (~5 cm) of microwave remote-sensors and the cost of maintaining high-density in-situ networks. Alternatively, data-driven techniques such as low-pass (LP) filters (exponential or moving-average) can generate a dimensionless index that mimics θ_{RZ} by smoothing the temporal variability in surface soil moisture (θ_S). The exponential filter approach (Albergel et al., 2008; Wagner et al., 1999) is used in several studies across point-scale (Bouaziz et al., 2020; Manfreda et al., 2014; Rossini & Patrignani, 2021) and remote-sensing scale (Bisselink et al., 2011; Brocca et al., 2011; Ford et al., 2014). Koster et al. (2023) used a LP filter on watershed-scale θ_S to demonstrate the potential of remotely sensed soil moisture observations to improve seasonal streamflow forecast skill.

Methodology: Vinit Sehgal, Binayak P. Mohanty, Rolf H. Reichle
Project administration: Binayak P. Mohanty
Resources: Vinit Sehgal, Binayak P. Mohanty
Software: Vinit Sehgal
Supervision: Binayak P. Mohanty
Validation: Vinit Sehgal, Binayak P. Mohanty
Visualization: Vinit Sehgal, Binayak P. Mohanty
Writing – original draft: Vinit Sehgal
Writing – review & editing: Binayak P. Mohanty, Rolf H. Reichle

While parametrically parsimonious, θ_{RZ} estimation from LP-filtered θ_S is limited by the scarcity of θ_{RZ} measurements to calibrate such filters. The use of model simulations for LP filter calibration (Liu et al., 2023; Tobin et al., 2019; Yang et al., 2022) can only mimic the functional relationships encoded a-priori in the models. Significant inter-model disagreement is common due to differences in the treatment of subgrid-scale heterogeneity in soil/vegetation properties (Qiu et al., 2020), exacerbated by the risk of equifinality during model calibration (Bouaziz et al., 2020; Boer-Euser et al., 2016). Moreover, the "*active*" rootzone layer, that is, the preferential depth for root-water uptake and land-atmospheric interactions, displays significant spatial variability owing to a combination of climate (temperature, net radiation and precipitation patterns), vegetation (rooting patterns, and preferential water uptake depth), and landscape characteristics, such as albedo and soil type (Feldman et al., 2024; Guswa, 2008; Jayawickreme et al., 2008; Milly, 2001). In contrast, most LSMs assume a fixed rootzone depth (typically, 1–2 m).

Terrestrial water and energy fluxes are strongly coupled at the landscape-scale through dynamic soil-vegetation-atmosphere interactions (Koster et al., 2023; Seneviratne et al., 2010; Zeppetello et al., 2019). The relationship between evaporative fraction (EF, ratio of actual and potential evapotranspiration) and θ_{RZ} manifests in two (Budyko) regimes and can be approximated as a piecewise-linear function (Figure 1a), constrained by the rootzone soil hydrologic regime thresholds. Knowing that *(a)* the temporal variability in the landscape-scale evaporative losses is moderated by the hydrologic state of θ_{RZ}, and *(b)* the temporal dynamics of θ_{RZ} can be mimicked by LP filtered θ_S; we hypothesize that the LP filter effect of the soil over θ_S is inherently engrained in the coupling dynamics of the terrestrial water and energy fluxes. Hence, the question arises– *Can the temporal dynamics of θ_{RZ} be reliably estimated using terrestrial water-energy coupling (WEC) principles together with θ_S and EF measurements*?

We develop a data-driven approach for estimating the active rootzone degree of saturation (S_{RZ} [–]) to mimic the temporal θ_{RZ} dynamics using θ_S observations from in-situ or Soil Moisture Active Passive (SMAP) satellite measurements, and EF from the Moderate Resolution Imaging Spectroradiometer (MODIS). As an extension, we generate rootzone soil moisture stress (SMS_{RZ}) as an indicator of drought stress on soil and vegetation, based on the instantaneous hydrologic state of θ_{RZ} relative to the hydrologic regime thresholds– both measured in terms of S_{RZ}.

2. Data

2.1. Soil Moisture Observations From SMAP and Sparse In-Situ Networks

We use volumetric surface (0–5 cm) soil moisture (m^3/m^3) from the SMAP Level-3 Soil Moisture Enhanced (SPL3E, version 5, 9 km gridded) product from 31st March 2015 to 31st December 2021. SMAP uses an L-band (1.41 GHz) microwave radiometer (Entekhabi et al., 2014; O'Neill et al., 2021), with 2–3 days revisit interval. The effect of diurnal variability in satellite retrievals is reduced by temporal thinning of θ_S to a uniform 1 day retrieval frequency as used by McColl et al. (2017) and Sehgal et al. (2020). SPL3E data flags (high vegetation water content, urban areas, large water bodies, precipitation, snow cover, etc.) are recorded during the analysis and are provided as an ancillary field with S_{RZ} estimates. The daily mean of ascending and descending overpasses from January 2022 through March 2023 is used for operational simulations of SMS_{RZ} (with a 2 day latency). The SMAP Level-4 Soil Moisture (SPL4) product (version 7, Reichle et al., 2022) provides global, 9 km gridded, 3 hourly mean volumetric soil moisture for the 0–100 cm layer (θ_{100}), which was averaged to daily values. SPL4 is generated using the Global Earth Observing System (GEOS) land data assimilation system, which ingests SMAP Level-1 brightness temperature into the Catchment land surface model, driven by meteorological forcings from the GEOS atmospheric data assimilation system and observation-corrected precipitation.

Daily in-situ volumetric soil moisture is obtained from the US Climate Reference Network (USCRN, Bell et al., 2013) and the Soil Climate Analysis Network (SCAN, Schaefer et al., 2007) at depths of 5, 10, 20, 50, and 100 cm. In-situ observed θ_{100} is calculated using the weighted average of records from the five measurement depths (details in the Supplement).

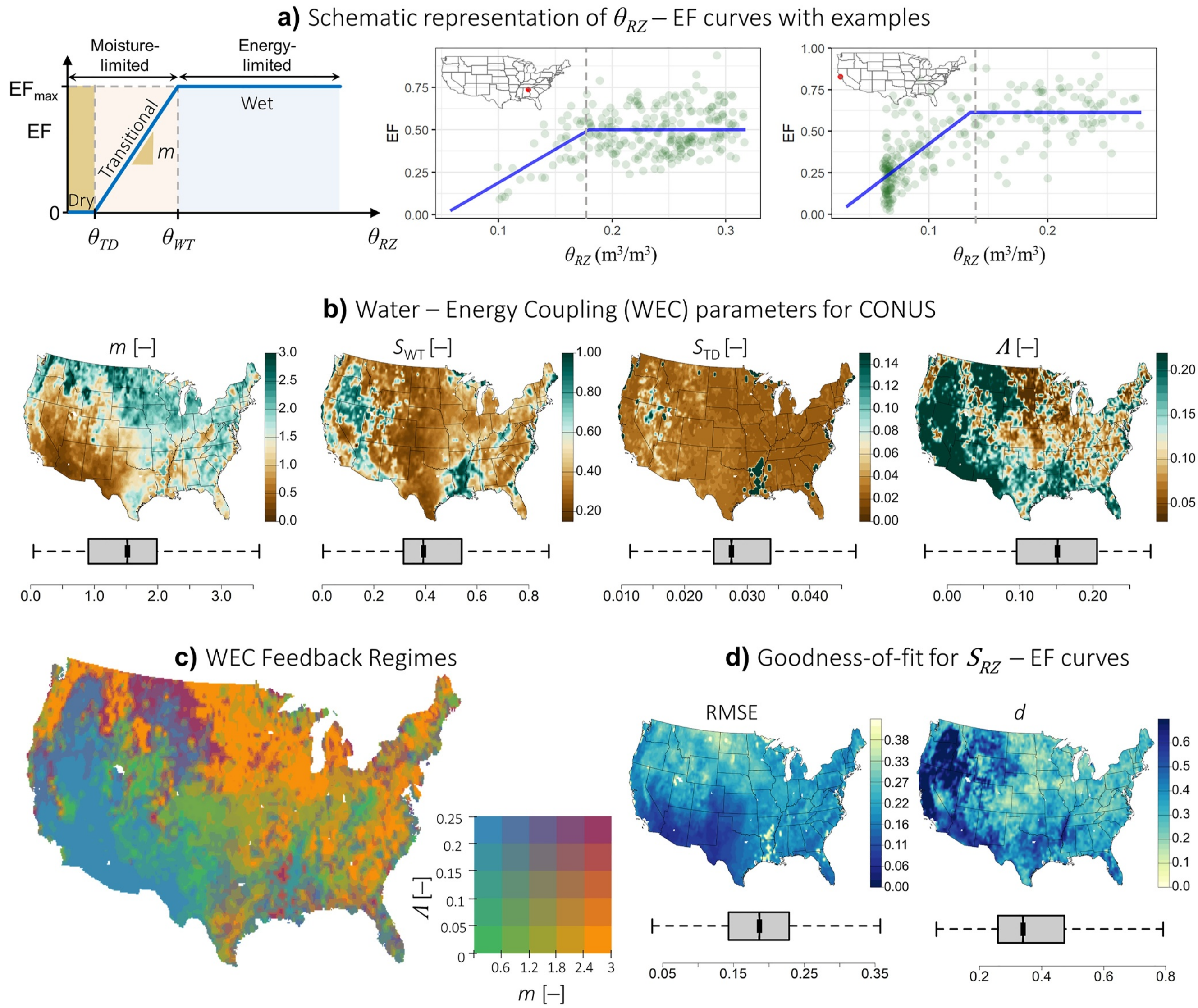

Figure 1. (a) Thematic representation of the WEC regimes, with sample plots at two in-situ locations (indicated by red dots in the inset maps) in contrasting hydroclimates. (b) WEC parameters (S_{TD}, S_{WT}, m, and Λ; all unitless). (c) WEC feedback regimes (d) RMSE and d for the fitted S_{RZ} − EF curves.

2.2. Potential and Actual Evapotranspiration

Gap-filled, eight-day composite total evapotranspiration (ET, in kg/m^2) is accessed from MODIS (MOD16A2GF, Version 6.1, Mu et al., 2011) for the period and extent matching SPL3E. MODIS uses the Penman−Monteith equation (Monteith, 1965; Penman, 1948) for estimating ET from daily meteorological reanalysis data and remotely sensed vegetation characteristics (Mu et al., 2011). MODIS ET and PET are bilinearly resampled to the 9 km SPL3E grid. For analysis at USCRN and SCAN sites, ET and PET are used at their 500 m (native) resolution, representing landscape-scale EF dynamics surrounding the soil node.

2.3. Drought Metrics

For comparison, we use drought severity maps from the U.S. Drought Monitor (USDM, Svoboda et al., 2002) and 30 day Evaporative Demand Drought Index (EDDI-30, Hobbins et al., 2016; McEvoy et al., 2016) and Standardized Precipitation Evapotranspiration Index (SPEI-30, Beguería et al., 2014; Vicente-Serrano et al., 2010) data based on the 4 km Gridded Surface Meteorological (gridMET) product (Abatzoglou, 2013).

3. Methodology

3.1. Low-Pass (LP) Filter Design and Rootzone Degree of Saturation, S_{RZ}

Under hydrologic equilibrium, the analytical solution of the 1-dimensional vertical water balance (differential) equation can be approximated using the relationship between the temporal θ_{RZ} changes and the difference between θ_S and the antecedent rootzone conditions (Albergel et al., 2008; Manfreda et al., 2014; Wagner et al., 1999). A simple recursive exponential LP filter to simulate the 1-dimensional first-order infinite-impulse response of θ_{RZ} to temporal variability in θ_S is given as:

$$\theta'_t = \theta'_{t-1} + \Lambda\left(\theta_{S,t} - \theta'_{t-1}\right), \qquad t \geq 1;\ \text{at}\ t = 1, \theta'_{t=0} = \theta_{S,t=0} \tag{1}$$

where, t = time [days], θ' = temporally smoothed (filtered) θ_s [m^3/m^3], Λ = exponential filter smoothing factor [–]; $\Lambda \in [0,1]$

The resulting θ' provides a first-order approximation of rootzone soil moisture dynamics under the assumption that lateral moisture flux to/from the rootzone is negligible, which is reasonable when the groundwater table is significantly deeper than the rootzone depth. Equation 1 yields the exponential weighted average (details in supplementary material, Section S2 in Supporting Information S1) of the antecedent observations using weights that are proportional to the terms of the geometric progression: 1, $(1 - \Lambda)$, $(1 - \Lambda)^2$, … $(1 - \Lambda)^n$, which is the discrete form of an exponential function (Hunter, 1986; Perry, 2010). This approach is advantageous because the periodicity in the hydrologic connections between θ_{RZ} and ET at the RS-footprint is often unknown, and can range from a few days (for barren or grassland landscapes) to seasonal scale (for deep-rooted vegetation) based on environmental conditions.

Temporal variability in θ' for a location with a smaller Λ is less responsive to recent θ_S changes (greater filtering of surface temporal variability), and vice-versa. Here, Λ is assumed to be time invariant. Λ controls the degree of attenuation and delay in θ' relative to surface conditions and is related to the e-folding time (τ) of the exponential filter as $\Lambda = 1 - e^{\frac{-\Delta t}{\tau}}$, where Δt is the temporal resolution of θ_s. For each pixel/location, Λ is assumed to represent the *effective* influence of various bio-geo-physical controls such as vegetation, topography, hydroclimatology and pedological characteristics (soil profile thickness, effective soil hydraulic characteristics, etc.) on vertical fluxes between the soil surface and the rootzone.

Since we make no explicit considerations to bias-correct θ' to the dynamic range of true θ_{RZ}, we normalize θ' to [0,1] to obtain S_{RZ}, a standardized measure of the θ_{RZ} hydrologic state, as:

$$S_{RZ,t} = \frac{\theta'_t - \theta'_{min}}{\theta'_{max} - \theta'_{min}} \tag{2}$$

Similarly, θ_{100} from SPL4 and in-situ stations is normalized to [0,1] for comparison with S_{RZ}, and is denoted as S_{100}.

3.2. Terrestrial Water-Energy Coupling

Terrestrial WEC regimes can be explained through a piece-wise linear function (Laio et al., 2001) between S_{RZ} and EF at time t as:

$$EF_t = \frac{ET_t}{PET_t} = \begin{cases} 0 & S_{RZ,t} \leq S_{TD} \\ m(S_{RZ,t} - S_{TD}) & S_{TD} < S_{RZ,t} < S_{WT} \\ m(S_{WT} - S_{TD}) & S_{RZ,t} \geq S_{WT} \end{cases} \tag{3}$$

Here, S_{WT} is the *effective* critical point, which refers to the threshold value of S_{RZ} at which the pixel transitions from energy-limited to moisture-limited conditions.

During wet soil conditions ($S_{RZ,t} > S_{WT}$), the system is in an energy-limited (Stage I ET) state, where the atmospheric moisture demand is satisfied by moisture-excess conditions. As the soil dries, the soil-vegetation-atmosphere system enters a water-limited state (Stage II ET), where soil moisture is the dominant source of daily temporal variability in ET. In Stage II, a positive land-atmospheric feedback is reached, whereas subsequent loss in soil moisture increases the land-surface temperature (thereby increasing PET). This supports moisture loss from the soil, albeit at a decreasing rate. The pixel enters the dry regime when $S_{RZ} \leq S_{TD}$, where S_{TD} is the *effective* wilting point of the pixel. The pixel maintains a transitional regime when $S_{TD} < S_{RZ} < S_{WT}$.

3.3. Parameter Optimization and Uncertainty Quantification

Equations 1–3 are implemented to optimize $\{S_{TD}, S_{WT}, m, \Lambda\}$ in an iterative framework using particle swarm optimization (PSO, Kennedy & Eberhart, 1995; Wang et al., 2018). The optimization minimizes the error function, ξ (with a tolerance threshold of 0.001), given as,

$$\xi = \sum_{t=1}^{N} \frac{|EF_{e,t} - EF_{o,t}|}{N} \tag{4}$$

where, $EF_{o,t}$ is the observed EF from MODIS at time t, $EF_{e,t}$ is the WEC-based estimated EF at time t, N = number of EF observations.

The root-mean-square error (RMSE) and Willmott's index of agreement ($d \in [0,1]$; Willmott et al., 2012) are used as goodness-of-fit (GOF) indicators of the fitted $S_{RZ} - EF$ curves. Higher values of d and lower values of RMSE indicate better $EF_o - EF_e$ agreement.

Model uncertainty is quantified using a drydown-based resampling and cross-validation where time-continuous resampling is used for ensemble model development (details in Section S2 in Supporting Information S1, supplementary material). For each ensemble run, the optimized WEC parameters (S_{TD}, S_{WT}, m, and Λ), θ'_{min} and θ'_{max} are stored. This facilitates a seamless conversion of future θ_s observations to equivalent S_{RZ} values in operational mode. SPL3E and EF pairs for each 36 km pixel (matching SMAP Level-3) are used for the development of the WEC parameters to ensure sufficient data samples for $S_{RZ} - EF$ models. The estimated WEC parameters are later resampled back to the SPL3E 9 km grid using bilinear interpolation.

3.4. Rootzone Soil Moisture Stress

We introduce θ_{RZ} stress ($\mathrm{SMS_{RZ}}$ $[-] \in [0,1]$), which captures the transition of the rootzone soil wetness from the energy-limited ($S_{RZ} > S_{WT}$, no stress) to the dry state ($S_{RZ} < S_{TD}$, maximum stress). $\mathrm{SMS_{RZ}}$ follows a non-linear, sigmoid relationship with S_{RZ}, following Sehgal et al., 2021, as given by Equation 6:

$$SMS_{RZ,t} = \frac{1}{1 + \left(\frac{S_{RZ,t}}{S_{IP}}\right)^2} \tag{5}$$

$$S_{IP} = \left(\frac{S_{WT} + S_{TD}}{2}\right) \tag{6}$$

The inflection point, S_{IP}, in the $S_{RZ} - SMS_{RZ}$ curve occurs when $S_{RZ} = S_{IP}$ and $SMS_{RZ} = 0.5$ $[-]$. The sensitivity of SMS_{RZ} to S_{RZ} is moderated by the exponent, which is fixed at 2.

4. Results and Discussion

4.1. Spatial Patterns of WEC Parameters and Land-Atmosphere Feedback Regimes

The spatial distributions of the WEC parameters and the GOF of the $S_{RZ} - EF$ curves over the Contiguous U.S. (CONUS) are shown in Figure 1b–1d. The relative availability of moisture and energy in the soil-vegetation-atmosphere continuum regulates the spatial patterns of m. The temporal variability in EF can be ~1.5 times (areal median) that of S_{RZ} and decreases as aridity increases. High rootzone water storage in wetter climates (e.g., Midwest, and Northeastern U.S.) supports a strong vegetation-atmosphere coupling through high transpiration and canopy evaporation (Williams & Torn, 2015; Zscheischler et al., 2015), contributing to higher m. The magnitude of PET in (hyper) arid climates is significantly higher than the actual soil evaporation or transpiration. Here, despite soil moisture being the dominant control of the daily temporal variability in ET (Akbar et al., 2018; Sehgal et al., 2020), the control of θ_{RZ} (or S_{RZ}) over EF is observed to be lower than previously reported by reanalysis or model data-based studies, such as Schwingshackl et al., 2017.

Lower Λ values are observed over the U.S. corn belt, where silty loam or loamy soils lead to slower infiltration rates than in the typical sandier soils of (hyper-) arid climates (Kumar et al., 2019). Higher S_{WT} values overlap with (semi-) arid regions, demonstrating preferentially dry hydrologic states (Sehgal & Mohanty, 2024), which contributes to the transition to an energy-limited regime at a higher S_{RZ}. Regions with intermediate WEC regimes (and bistable soil moisture states) typically have $S_{WT} < 0.5$, that is, the dynamic soil moisture range shows a near-equal distribution of energy- and moisture-limited states. For arid regions with sandy soils, the change from transitional to dry state (at S_{TD}) occurs at a higher soil moisture. This rapid desiccation of the coarse-textured surface soil plays an important ecological function (through inverse texture effect) by preventing moisture loss from the deeper layers (Fernandez-Illescas et al., 2001). For most other parts of CONUS, S_{TD} is observed to be close to the lower extreme of the dynamic range of S_{RZ}.

The spatial distribution of Λ (i.e., $\theta_S - \theta_{RZ}$ response relationship) and m ($\theta_{RZ} - EF$ interactions) reflects mesoscale soil-vegetation-climate interactions and WEC feedbacks (Figure 1c). In (hyper) arid climates, sparse vegetation, coarse-textured soils, and high PET yield high soil evaporation rates. Land-atmospheric interactions in such regions are governed by negative WEC feedback, where increased soil moisture loss leads to warming and drying of the atmospheric boundary layer, resulting in further increase in PET, and lower EF (Gentine et al., 2019). These regions are characterized by a rapid loss of moisture pulse from shallower profiles, as captured by high Λ and low m. In contrast, in humid and sub-humid regions, a larger fraction of atmospheric moisture demand is satisfied by ET (high m). Here, an increase in ET cools the atmospheric boundary layer, reduces PET and increases EF—thereby establishing a negative feedback mechanism. Lower values of Λ over these regions are the result of the deep-rooted vegetation sustaining high transpiration rates over long periods (despite drying of the surface layer). Grasslands in the Central Great Plains show intense transpiration rates immediately following a moisture pulse, followed by a drought-induced dormancy (Williams & Torn, 2015) which contributes to longer time scales of SM-EF coupling (low Λ). Differences in the plant functional type and phenological characteristics impact the preferential depths of root water uptake (Feldman et al., 2024) and can significantly impact the overall Λ– m relationship.

Interestingly, positive and negative WEC feedback regimes align, respectively, with the dry and wet-preferential hydrologic states of soil moisture (Sehgal & Mohanty, 2024). The intermediate regions display a bistable hydrologic state, where complementary tipping mechanisms dictate dynamic changes in the WEC state from energy-limited to moisture-limited, and vice-versa. Hence, while the $S_{RZ} - EF$ coupling is primarily a climate-controlled process, the relative state of soil moisture and vegetation characteristics dictates WEC feedback processes and the intensity, duration, and frequency of the transition between WEC regimes. This highlights the coevolution and coexistence of soil-vegetation-climate through complementary and constrained processes.

The shallow groundwater table and rapid infiltration owing to shallow fractured-rock aquifers over the Mississippi alluvial plains—a phenomenon also observed in the US southwest coastal plains (Shapiro & Falcone, 2022; Zell & Sanford, 2020)—overlaps with unusually high values of S_{WT} and S_{TD}, and low m. Widespread irrigation in the Mississippi alluvial plains further contributes in altering the landscape evaporative regimes by reducing the land-surface temperature (Chen & Dirmeyer, 2019), thereby reducing S_{RZ} controls over EF, which is reflected in low m values.

Significant seasonal changes in the landscape characteristics (snow-cover and/or frozen ground during winter, and dramatic changes in the grassland biomass and productivity during spring) in the higher latitudes, including the Northern Great Plains and US Northeast, may lead to seasonal variability in the $S_{RZ} - EF$ characteristics as reflected in the higher fitting RMSE (Figure 1d). Preference is given to the RMSE statistic in adjudicating the fitting accuracy of the $S_{RZ} - EF$ curves (see Section S3 in Supporting Information S1), which are deemed satisfactory over CONUS with a median value of 0.14 [−].

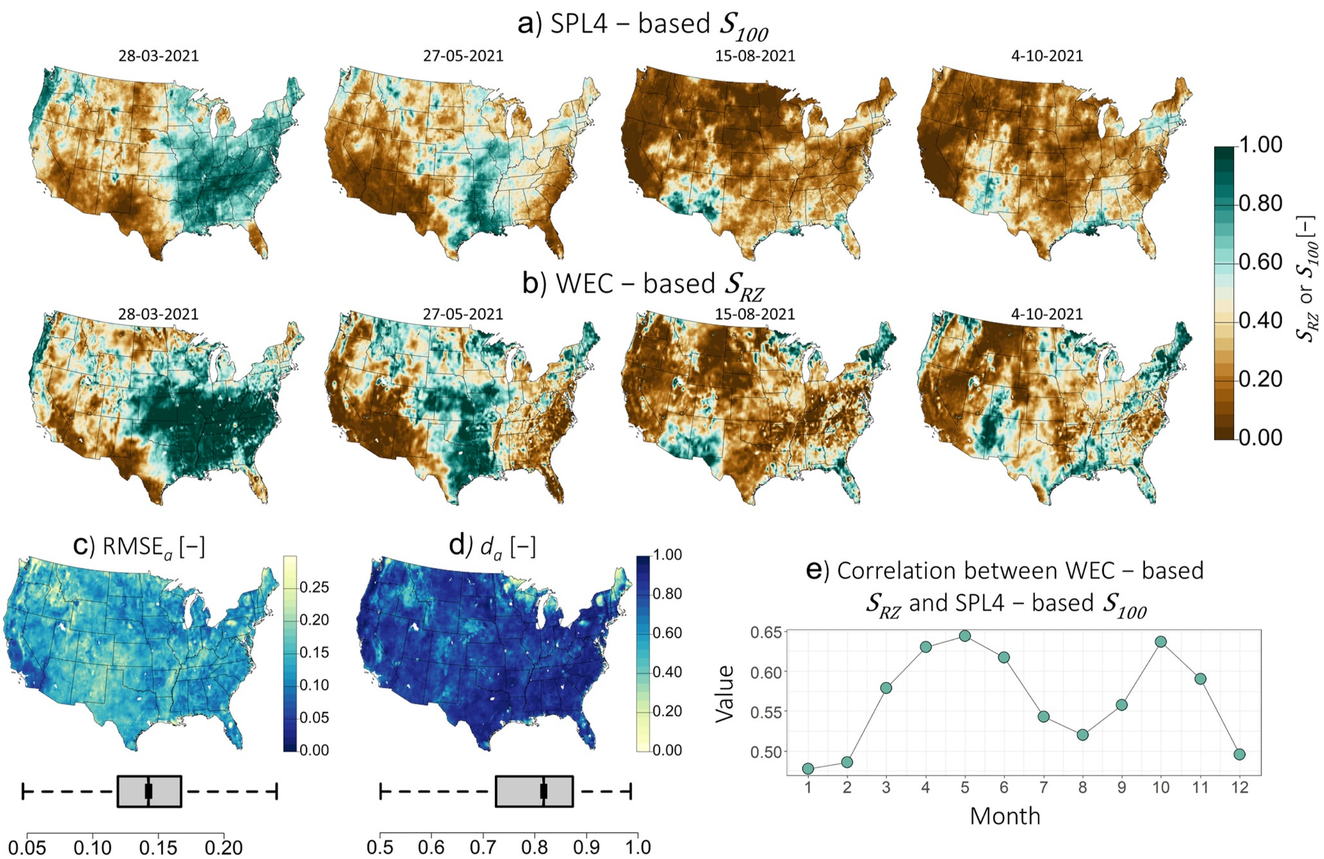

Figure 2. (a–b) S_{RZ} (from WEC) and S_{100} (from SPL4) for select dates (c–d) RMSE$_a$ and d_a between S_{RZ} and S_{100} anomalies (computed after removing seasonal means; details in supplementary material). (e) Areal median of the seasonal S_{RZ} versus S_{100} correlation.

4.2. *Validation of WEC-Based S_{RZ}* Across CONUS

A comparison between WEC-based S_{RZ} estimates with S_{100} from SPL4 shows strong spatio-temporal agreement (Figures 2a and 2b). RMSE and d between the S_{RZ} and S_{100} anomalies (RMSE$_a$ and d_a, details in the supplementary material) are observed to be satisfactory across CONUS, with a median RMSE$_a$ of 0.14 and d_a of 0.82 (Figures 2c and 2d). Correlation between the two datasets shows a seasonal trend (Figure 2e and Figure S2 in Supporting Information S1) with areal-median $R = 0.45$ [−] in January, 0.65 [−] in May, and 0.52 [−] in August. The drop in the S_{RZ} versus S_{100} correlation in winter is primarily driven by increased uncertainty in WEC-based EF estimates over Central/Northern plains as previously discussed (Figure 1d). In contrast, θ_S in the arid regions of the Southwestern U.S. (Mojave, Sonora and Baja Deserts, for example) may decorrelate from the rootzone during summer, while temporal variability in EF may, instead, be regulated by vapor diffusion and transpiration from deep soil profiles by the xeric vegetation (Stocker et al., 2023). In contrast, SPL4 uses a fixed 1 m rootzone thickness, which leads to differences in the estimated rootzone soil moisture dynamics in the two datasets. This indicates a potential limitation of temporally invariant Λ in representing space-time variability in the land-atmospheric interactions governing the true $S_{RZ} - EF$ relationship across different hydroclimates. A temporally invariant $S_{RZ} - EF$ pathway ignores the seasonal variability in the WEC dynamics owing to the complex, nonlinear micrometeorological processes and resultant changes in the radiative, thermal and kinetic energy balance of land-atmospheric interaction (Haghighi et al., 2018; Hsu & Dirmeyer, 2023). Such factors may cause a shift in the critical thresholds of the WEC regimes, as reported by Hsu & Dirmeyer, 2023. It is noteworthy that SPL4 employs explicit parameterization of actual rooting depth, and seasonally varying vegetation control on transpiration, which further adds to the model complexity and error sources. The overall performance of the S_{RZ} estimates from the WEC-based approach is similar to those of S_{100} estimates derived from LP filter parameters trained with the in-situ observed θ_{100} at USCRN/SCAN stations (Figure 3). GOF for the WEC-based S_{RZ} estimates is satisfactory, with median unbiased RMSE = 0.044 [−], $d = 0.76$ [−] and $R = 0.8$ [−]. While both the

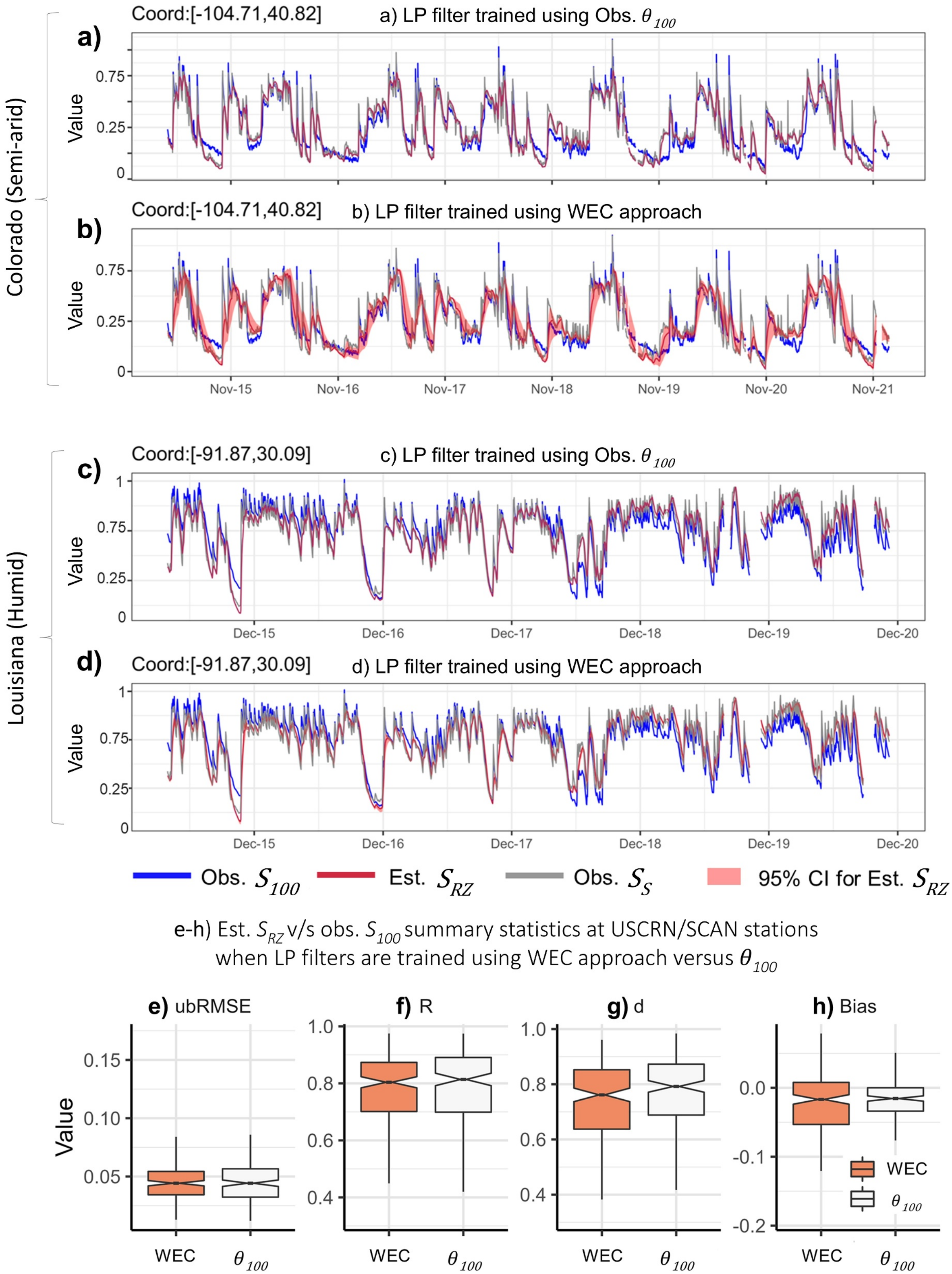

Figure 3. Estimated S_{RZ} (red line) using the LP filter calibrated with (a),(c) in-situ observed θ_{100} and (b),(d) the WEC-based approach, for locations in (a),(b) Colorado (semi-arid) and (c),(d) Louisiana (humid). The observed S_S (gray line) and S_{100} (blue line) are θ_S and θ_{100} normalized to a range [0,1] (e)–(h) GOF summary of the estimated S_{RZ} at the USCRN/SCAN stations ($n = 218$) generated with θ_{100} and WEC-based LP filters. Spatial maps of the seasonal statistics are provided in Figure S3 in Supporting Information S1 of the supplementary material.

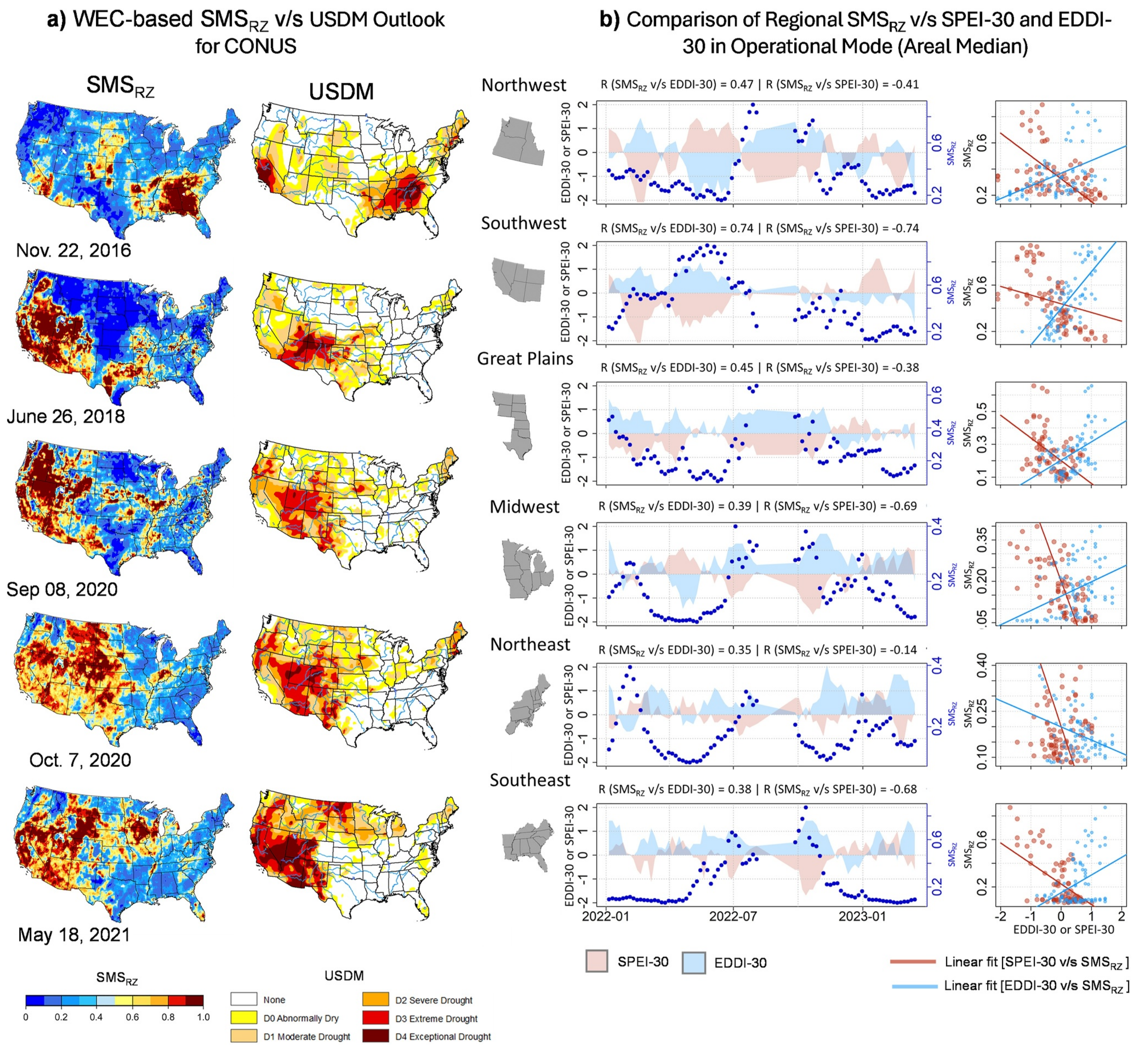

Figure 4. (a) SMS$_{RZ}$ and USDM outlook for select dates. (b) Time series and scatterplot of areal-median SMS$_{RZ}$ (blue dots), EDDI-30 (light blue) and SPEI-30 (light red) for six CONUS regions (following the Fifth National Climate Assessment report, Jay et al., 2023). August 2022 values of SMS$_{RZ}$ (blue) are missing because SMAP was in safe mode.

WEC and observed θ_{100}-based LP filters show a negative bias in estimating S_{RZ}, the overall bias of WEC-based S_{RZ} is marginally higher (median value of -0.017) owing to the random error associated with the $S_{RZ} - EF$ curves parameterization.

4.3. Operational Near-Real-Time Agricultural Drought Monitoring Using WEC-Based S_{RZ}

The thresholds of the WEC regimes facilitate daily, operational near-real-time SMS$_{RZ}$ estimation using θ_S for agricultural drought impact monitoring. A retrospective comparison between SMS$_{RZ}$ and the US Drought Monitor (USDM, Svoboda et al., 2002) for select dates (Figures 4a and 4b) shows a general agreement between the two datasets for droughts in the US Southeast (November 2016), Great Plains and Western U.S. (October 2020), and Midwestern and Southwestern U.S. (May 2021), among others. The analysis is extended in operational mode using θ_S from SLP3E (with 2 day latency), which captures drought stress over the U.S. Southwest (Summer

2022), Northwest and Southeastern U.S., and Great Plains (fall, 2022). The areal median SMS_{RZ} for six CONUS regions show statistically significant positive (negative) correlation with 30 day EDDI (SPEI) (Figure 4c) ranging from 0.74 (−0.74) for the US Southwest, and relatively low values of 0.35 (−0.14) for the Northeastern US. Since the (linear) correlation-based assessment ignores the non-linear interactions between SMS_{RZ} and meteorological variables such as ET, the true temporal association between these indices might be higher.

Differences in SMS_{RZ} (soil hydrologic state vis-à-vis WEC thresholds) and climatology-based drought indices (deviation from long-term normals) may occur due to the differing definition of drought. For example, climatologically normal warm and dry conditions during summer in the Southwestern US, may not be categorized as a drought in terms of long-term anomalies, while SMS_{RZ} may indicate high stress for the region due to sustenance of water-limited hydrologic conditions. Horizontal fluxes may not be negligible in regions with shallow groundwater, thereby invalidating one of the key assumptions of the piecewise-linear WEC framework. SMS_{RZ} estimates in such cases may overestimate drought severity as it doesn't account for the θ_{RZ}-groundwater interactions. Therefore, an understanding of regional hydrology is important to correctly interpret SMS_{RZ} for decision making.

5. Conclusion

Despite advancements in remote-sensing techniques for retrieving θ_S, accurate estimation of θ_{RZ} dynamics remains a challenge. We use satellite-based EF and θ_S to design a LP filter to estimate active rootzone soil moisture dynamics (as S_{RZ} [−]) through a constrained optimization of the pixel-scale WEC pathway ($S_{RZ} - EF$). This addresses the challenge posed by sparse coverage of in-situ θ_{RZ} observations to calibrate the LP filters to model/monitor space-time contiguous, continental-scale dynamics of θ_{RZ}.

The accuracy of the proposed approach in estimating θ_{RZ} dynamics is comparable to LP filters parameterized using in-situ observed rootzone soil moisture. We use this methodology to develop spatiotemporal fields of S_{RZ} at 9 km spatial resolution for CONUS, which displays a high degree of agreement with a similar index generated from the SPL4 product. The advantage of simultaneous parameterization of the WEC pathway and LP filter is the availability of the critical thresholds of water-limited and energy-limited regimes. This facilitates the translation of S_{RZ} to SMS_{RZ}—an indicator of drought impacts on soil and vegetation—which is demonstrated as a tool to generate low-latency (2 day), daily, spatially continuous updates of agricultural drought impact across CONUS.

Data Availability Statement

SMAP soil moisture, MODIS PET and ET data is available at NASA National Snow, and Ice Data Center Distributed Active Archive Center (NSIDC-DAAC, https://nsidc.org/data/data-programs/nsidc-daac). The Water-Energy Coupling parameters generated in this study are available in raster format (9 × 9 km^2 grids) on HydroShare through Sehgal and Mohanty (2023). US Climate Reference dataset is accessed through: https://www.ncei.noaa.gov/access/crn/. SCAN dataset is available through: https://www.drought.gov/data-maps-tools/soil-climate-analysis-network-scan. EDDI-30 and SPEI-30 data is accessed from GridMet webpage at https://www.climatologylab.org/gridmet.html. USDM drought outlook is accessed from: https://droughtmonitor.unl.edu/.

Acknowledgments
Funding support from NASA-SMAP projects (NNX16AQ58G, 80NSSC20K1807) is gratefully acknowledged.

References

Abatzoglou, J. T. (2013). Development of gridded surface meteorological data for ecological applications and modelling. *International Journal of Climatology*, *33*(1), 121–131. https://doi.org/10.1002/joc.3413

Akbar, R., Short Gianotti, D. J., McColl, K. A., Haghighi, E., Salvucci, G. D., & Entekhabi, D. (2018). Estimation of landscape soil water losses from satellite observations of soil moisture. *Journal of Hydrometeorology*, *19*(5), 871–889. https://doi.org/10.1175/jhm-d-17-0200.1

Albergel, C., Rüdiger, C., Pellarin, T., Calvet, J.-C., Fritz, N., Froissard, F., et al. (2008). From near-surface to root-zone soil moisture using an exponential filter: An assessment of the method based on in-situ observations and model simulations. *Hydrology and Earth System Sciences Discussions*, *5*(3), 1603–1640. https://doi.org/10.5194/hessd-5-1603-2008

Beguería, S., Vicente-Serrano, S. M., Reig, F., & Latorre, B. (2014). Standardized precipitation evapotranspiration index (SPEI) revisited: Parameter fitting, evapotranspiration models, tools, datasets and drought monitoring. *International Journal of Climatology*, *34*(10), 3001–3023. https://doi.org/10.1002/joc.3887

Bell, J. E., Palecki, M. A., Baker, C. B., Collins, W. G., Lawrimore, J. H., Leeper, R. D., et al. (2013). U.S. climate reference network soil moisture and temperature observations. *Journal of Hydrometeorology*, *14*(3), 977–988. https://doi.org/10.1175/JHM-D-12-0146.1

Bisselink, B., Van Meijgaard, E., Dolman, A. J., & De Jeu, R. A. M. (2011). Initializing a regional climate model with satellite-derived soil moisture. *Journal of Geophysical Research*, *116*(2), 1–13. https://doi.org/10.1029/2010JD014534

Bouaziz, L. J. E., Steele-Dunne, S. C., Schellekens, J., Weerts, A. H., Stam, J., Sprokkereef, E., et al. (2020). Improved understanding of the link between catchment-scale vegetation accessible storage and satellite-derived soil water index. *Water Resources Research*, *56*(3), 1–22. https://doi.org/10.1029/2019WR026365

Brocca, L., Hasenauer, S., Lacava, T., Melone, F., Moramarco, T., Wagner, W., et al. (2011). Soil moisture estimation through ASCAT and AMSR-E sensors: An intercomparison and validation study across Europe. *Remote Sensing of Environment*, *115*(12), 3390–3408. https://doi.org/10.1016/j.rse.2011.08.003

Chen, L., & Dirmeyer, P. A. (2019). Global observed and modelled impacts of irrigation on surface temperature. *International Journal of Climatology*, *39*(5), 2587–2600. https://doi.org/10.1002/joc.5973

Dash, C. J., Sarangi, A., Singh, D. K., & Adhikary, P. P. (2019). Numerical simulation to assess potential groundwater recharge and net groundwater use in a semi-arid region. *Environmental Monitoring and Assessment*, *191*(6), 371. https://doi.org/10.1007/s10661-019-7508-y

de Boer-Euser, T., McMillan, H. K., Hrachowitz, M., Winsemius, H. C., & Savenije, H. H. G. (2016). Influence of soil and climate on root zone storage capacity. *Water Resources Research*, *52*(3), 2009–2024. https://doi.org/10.1002/2015wr018115

Entekhabi, D., Yueh, S., O'Neill, P. E., Kellogg, K. H., Allen, A., Bindlish, R., et al. (2014). SMAP handbook--soil moisture active passive: Mapping soil moisture and freeze/thaw from space.

Feldman, A. F., Koster, R. D., Cawse-Nicholson, K., Crow, W. T., Holmes, T. R. H., & Poulter, B. (2024). Soil moisture profiles of ecosystem water use revealed with ECOSTRESS. *Geophysical Research Letters*, *51*(8). https://doi.org/10.1029/2024GL108326

Fernandez-Illescas, C. P., Porporato, A., Laio, F., & Rodriguez-Iturbe, I. (2001). The ecohydrological role of Soil texture in a water-limited ecosystem. *Water Resources Research*, *37*(12), 2863–2872. https://doi.org/10.1029/2000WR000121

Ford, T. W., Harris, E., & Quiring, S. M. (2014). Estimating root zone soil moisture using near-surface observations from SMOS. *Hydrology and Earth System Sciences*, *18*(1), 139–154. https://doi.org/10.5194/hess-18-139-2014

Gentine, P., Green, J. K., Guérin, M., Humphrey, V., Seneviratne, S. I., Zhang, Y., & Zhou, S. (2019). Coupling between the terrestrial carbon and water cycles - a review. *Environmental Research Letters*, *14*(8), 083003. https://doi.org/10.1088/1748-9326/ab22d6

Guswa, A. J. (2008). The influence of climate on root depth: A carbon cost-benefit analysis. *Water Resources Research*, *44*(2), 1–11. https://doi.org/10.1029/2007WR006384

Haghighi, E., Short Gianotti, D. J., Akbar, R., Salvucci, G. D., & Entekhabi, D. (2018). Soil and atmospheric controls on the land surface energy balance: A generalized framework for distinguishing moisture-limited and energy-limited evaporation regimes. *Water Resources Research*, *54*(3), 1831–1851. https://doi.org/10.1002/2017WR021729

Hobbins, M. T., Wood, A., McEvoy, D. J., Huntington, J. L., Morton, C., Anderson, M., & Hain, C. (2016). The evaporative demand drought index. Part I: Linking drought evolution to variations in evaporative demand. *Journal of Hydrometeorology*, *17*(6), 1745–1761. https://doi.org/10.1175/jhm-d-15-0121.1

Hsu, H., & Dirmeyer, P. A. (2023). Uncertainty in projected critical soil moisture values in CMIP6 affects the interpretation of a more moisture-limited world. *Earth's Future*, *11*(6). https://doi.org/10.1029/2023EF003511

Hunter, J. S. (1986). The exponentially weighted moving average. *Journal of Quality Technology*, *18*(4), 203–210. https://doi.org/10.1080/00224065.1986.11979014

Jay, A. K., Crimmins, A. R., Avery, C. W., Dahl, T. A., Dodder, R. S., Hamlington, B. D., et al. (2023). Overview: Understanding risks, impacts, and responses. In A. R. Crimmins, C. W. Avery, D. R. Easterling, K. E. Kunkel, B. C. Stewart, & T. K. Maycock (Eds.), *Fifth national climate assessment*. U.S. Global Change Research Program. https://doi.org/10.7930/NCA5.2023.CH1

Jayawickreme, D. H., van Dam, R. L., & Hyndman, D. W. (2008). Subsurface imaging of vegetation, climate, and root-zone moisture interactions. *Geophysical Research Letters*, *35*(18), 1–5. https://doi.org/10.1029/2008GL034690

Kennedy, J., & Eberhart, R. (1995). Particle swarm optimization. *Proceedings of ICNN'95-International Conference on Neural Networks*, *4*, 1942–1948. https://doi.org/10.1109/icnn.1995.488968

Koster, R. D., Liu, Q., Crow, W. T., & Reichle, R. H. (2023). Late-fall satellite-based soil moisture observations show clear connections to subsequent spring streamflow. *Nature Communications*, *14*(1), 1–7. https://doi.org/10.1038/s41467-023-39318-3

Kumar, S., Newman, M., Wang, Y., & Livneh, B. (2019). Potential reemergence of seasonal soil moisture anomalies in North America. *Journal of Climate*, *32*(10), 2707–2734. https://doi.org/10.1175/JCLI-D-18-0540.1

Laio, F., Porporato, A., Fernandez-Illescas, C. P., & Rodriguez-Iturbe, I. (2001). Plants in water-controlled ecosystems: Active role in hydrologic processes and response to water stress. *Advances in Water Resources*, *24*(7), 745–762. https://doi.org/10.1016/s0309-1708(01)00007-0

Li, G., Niu, W., Sun, J., Zhang, W., Zhang, E., & Wang, J. (2021). Soil moisture and nitrogen content influence wheat yield through their effects on the root system and soil bacterial diversity under drip irrigation. *Land Degradation & Development*, *32*(10), 3062–3076. https://doi.org/10.1002/ldr.3967

Lin, L., Band, L. E., Vose, J. M., Hwang, T., Miniat, C. F., & Bolstad, P. V. (2019). Ecosystem processes at the watershed scale: Influence of flowpath patterns of canopy ecophysiology on emergent catchment water and carbon cycling. *Ecohydrology*, *12*(5), 1–15. https://doi.org/10.1002/eco.2093

Liu, E., Zhu, Y., Lü, H., Horton, R., Gou, Q., Wang, X., et al. (2023). Estimation and assessment of the root zone soil moisture from near-surface measurements over huai river basin. *Atmosphere*, *14*(1), 124. https://doi.org/10.3390/atmos14010124

Manfreda, S., Brocca, L., Moramarco, T., Melone, F., & Sheffield, J. (2014). A physically based approach for the estimation of root-zone soil moisture from surface measurements. *Hydrology and Earth System Sciences*, *18*(3), 1199–1212. https://doi.org/10.5194/hess-18-1199-2014

McColl, K. A., Alemohammad, S. H., Akbar, R., Konings, A. G., Yueh, S., & Entekhabi, D. (2017). The global distribution and dynamics of surface soil moisture. *Nature Geoscience*, *10*(2), 100–104. https://doi.org/10.1038/ngeo2868

McEvoy, D. J., Huntington, J. L., Hobbins, M. T., Wood, A., Morton, C., Anderson, M., & Hain, C. (2016). The evaporative demand drought index. Part II: CONUS-Wide assessment against common drought indicators. *Journal of Hydrometeorology*, *17*(6), 1763–1779. https://doi.org/10.1175/JHM-D-15-0122.1

Milly, P. C. D. (2001). A minimalist probabilistic description of root zone soil water. *Water Resources Research*, *37*(3), 457–463. https://doi.org/10.1029/2000WR900337

Monteith, J. L. (1965). Evaporation and environment. *Symposia of the Society for Experimental Biology*, *19*, 205–234.

Mu, Q., Zhao, M., & Running, S. W. (2011). Improvements to a {MODIS} global terrestrial evapotranspiration algorithm. *Remote Sensing of Environment*, *115*(8), 1781–1800. https://doi.org/10.1016/j.rse.2011.02.019

O'Neill, P. E., Chan, S., Njoku, E. G., Jackson, T., Bindlish, R., Chaubell, J., & Colliander, A. (2021). SMAP enhanced L3 radiometer global and polar grid daily 9 km EASE-grid soil moisture, version 5. [DataSet]. Boulder, Colorado USA. https://doi.org/10.5067/4DQ54OUIJ9DL. *NASA National Snow and Ice Data Center Distributed Active Archive Center*.

Penman, H. L. (1948). Natural evaporation from open water, bare soil and grass. *Proceedings of the Royal Society of London - Series A: Mathematical and Physical Sciences*, *193*(1032), 120–145.

Perry, M. B. (2010). The exponentially weighted moving average. *Wiley Encyclopedia of Operations Research and Management Science*.

Qiu, J., Crow, W. T., Dong, J., & Nearing, G. S. (2020). Model representation of the coupling between evapotranspiration and soil water content at different depths. *Hydrology and Earth System Sciences*, *24*(2), 581–594. https://doi.org/10.5194/hess-24-581-2020

Raghav, P., & Kumar, M. (2021). Retrieving gap-free daily root zone soil moisture using surface flux equilibrium theory. *Environmental Research Letters*, *16*(10), 104007. https://doi.org/10.1088/1748-9326/ac2441

Reichle, R., De Lannoy, G., Koster, R. D., Crow, W. T., Kimball, J. S., Liu, Q., & Bechtold, M. (2022). SMAP L4 global 3-hourly 9 km EASE-grid surface and root zone soil moisture geophysical data. Version 7. [DataSet]. *NASA National Snow and Ice Data Center Distributed Active Archive Center* https://nsidc.org/sites/default/files/multi_spl4smau-v002-userguide_1.pdf

Rossini, P., & Patrignani, A. (2021). Predicting rootzone soil moisture from surface observations in cropland using an exponential filter. *Soil Science Society of America Journal*, *85*(6), 1894–1902. https://doi.org/10.1002/saj2.20319

Schaefer, G. L., Cosh, M. H., & Jackson, T. J. (2007). The USDA natural Resources conservation service soil climate analysis network (SCAN). *Journal of Atmospheric and Oceanic Technology*, *24*(12), 2073–2077. https://doi.org/10.1175/2007JTECHA930.1

Schwingshackl, C., Hirschi, M., & Seneviratne, S. I. (2017). Quantifying spatiotemporal variations of soil moisture control on surface energy balance and near-surface air temperature. *Journal of Climate*, *30*(18), 7105–7124. https://doi.org/10.1175/JCLI-D-16-0727.1

Sebastian, D. E., Murtugudde, R., & Ghosh, S. (2023). Soil–vegetation moisture capacitor maintains dry season vegetation productivity over India. *Scientific Reports*, *13*(1), 1–10. https://doi.org/10.1038/s41598-022-27277-6

Sehgal, V., Gaur, N., & Mohanty, B. P. (2020). Global surface soil moisture drydown patterns. *Water Resources Research*, *57*(1). https://doi.org/10.1029/2020WR027588

Sehgal, V., Gaur, N., & Mohanty, B. P. (2021). Global flash drought monitoring using surface soil moisture. *Water Resources Research*, *57*(9), 1–25. https://doi.org/10.1029/2021WR029901

Sehgal, V., & Mohanty, B. (2023). *Satellite-based terrestrial water-energy coupling parameters for CONUS*. HydroShare. Retrieved from http://www.hydroshare.org/resource/76b7021366b34f97b1da45c925ccd748

Sehgal, V., & Mohanty, B. P. (2024). Preferential hydrologic states and tipping characteristics of global surface soil moisture. *Water Resources Research*, *60*(4). https://doi.org/10.1029/2023WR034858

Seneviratne, S. I., Corti, T., Davin, E. L., Hirschi, M., Jaeger, E. B., Lehner, I., et al. (2010). Investigating soil moisture-climate interactions in a changing climate: A review. *Earth-Science Reviews*, *99*(3–4), 125–161. Elsevier. https://doi.org/10.1016/j.earscirev.2010.02.004

Shapiro, A. M., & Falcone, J. A. (2022). Mapping areas of groundwater susceptible to transient contamination events from rapid infiltration into shallow fractured-rock aquifers in agricultural regions of the conterminous United States.

Stocker, B. D., Tumber-Dávila, S. J., Konings, A. G., Anderson, M. C., Hain, C., & Jackson, R. B. (2023). Global patterns of water storage in the rooting zones of vegetation. *Nature Geoscience*, *16*(3), 250–256. https://doi.org/10.1038/s41561-023-01125-2

Svoboda, M., LeComte, D., Hayes, M., Heim, R., Gleason, K., Angel, J., et al. (2002). The drought monitor. *Bulletin of the American Meteorological Society*, *83*(8), 1181–1190. https://doi.org/10.1175/1520-0477-83.8.1181

Tobin, K. J., Crow, W. T., Dong, J., & Bennett, M. E. (2019). Validation of a new root-zone soil moisture product: Soil MERGE. *Ieee Journal of Selected Topics in Applied Earth Observations and Remote Sensing*, *12*(9), 3351–3365. https://doi.org/10.1109/JSTARS.2019.2930946

Vicente-Serrano, S. M., Beguería, S., & López-Moreno, J. I. (2010). A multiscalar drought index sensitive to global warming: The standardized precipitation evapotranspiration index. *Journal of Climate*, *23*(7), 1696–1718. https://doi.org/10.1175/2009JCLI2909.1

Wagner, W., Lemoine, G., & Rott, H. (1999). A method for estimating soil moisture from ERS Scatterometer and soil data. *Remote Sensing of Environment*, *70*(2), 191–207. https://doi.org/10.1016/S0034-4257(99)00036-X

Wang, D., Tan, D., & Liu, L. (2018). Particle swarm optimization algorithm: An overview. *Soft Computing*, *22*(2), 387–408. https://doi.org/10.1007/s00500-016-2474-6

Wang, J., Niu, W., Zhang, M., & Li, Y. (2017). Effect of alternate partial root-zone drip irrigation on soil bacterial communities and tomato yield. *Applied Soil Ecology*, *119*(26), 250–259. https://doi.org/10.1016/j.apsoil.2017.06.032

Williams, I. N., & Torn, M. S. (2015). Vegetation controls on surface heat flux partitioning, and land-atmosphere coupling. *Geophysical Research Letters*, *42*(21), 9416–9424. https://doi.org/10.1002/2015GL066305

Willmott, C. J., Robeson, S. M., & Matsuura, K. (2012). A refined index of model performance. *International Journal of Climatology*, *32*(13), 2088–2094. https://doi.org/10.1002/joc.2419

Yang, Y., Bao, Z., Wu, H., Wang, G., Liu, C., Wang, J., & Zhang, J. (2022). An exponential filter model-based root-zone soil moisture estimation methodology from multiple datasets. *Remote Sensing*, *14*(8), 1–22. https://doi.org/10.3390/rs14081785

Zell, W. O., & Sanford, W. E. (2020). Calibrated simulation of the long-term average surficial groundwater system and derived spatial distributions of its characteristics for the contiguous United States. *Water Resources Research*, *56*(8), 1–16. https://doi.org/10.1029/2019WR026724

Zeppetello, L. V. R., Battisti, D. S., & Baker, M. B. (2019). The origin of soil moisture evaporation "regimes.". *Journal of Climate*, *32*(20), 6939–6960. https://doi.org/10.1175/JCLI-D-19-0209.1

Zscheischler, J., Orth, R., & Seneviratne, S. I. (2015). A submonthly database for detecting changes in vegetation-atmosphere coupling. *Geophysical Research Letters*, *42*(22), 9816–9824. https://doi.org/10.1002/2015GL066563